Pergamon

Int. J. Heat Mass Transfer. Vol. 37, Suppl. 1, pp. 333–346, 1994

0017-9310/94 $6.00 + 0.00

0017-9310(93)E0054-K

Heat transfer from a planar surface to a fluid in laminar flow. An experimental and computational study

J. F. T. PITTMAN, J. F. RICHARDSON, A. O. SHARIF and C. P. SHERRARD†

Department of Chemical Engineering, University College, Swansea SA2 8PP, U.K.

Abstract—An experimental study has been made of heat transfer from a flat plate with nominally uniform surface heat flux aligned parallel to laminar flows of Newtonian and shear thinning liquids, for a range of plate Reynolds numbers (30–2000) and fluid Prandtl numbers (50–400). Finite element solutions of the coupled flow and conjugate heat transfer problem have been obtained, using a recent form of the SUPG formulation for isoparametric biquadratic finite elements, extended to take account of variable physical properties. Close agreement with experimental plate surface temperatures provides confidence in both our experimental and numerical techniques.

1. INTRODUCTION

THE SUBJECT of the paper is an experimental and computational project on heat transfer from surfaces immersed in fluids in laminar flow. The emphasis is on liquids of high viscosity, some with non-Newtonian flow properties, many of which exhibit variations of consistency and density with temperature—conditions which are relevant in many industrially important processes involving polymeric liquids and solutions, suspensions and emulsions. The nonlinearity of the coupled momentum and energy conservation equations which apply in this situation renders an analytical treatment impossible, except in certain special cases. Fluid consistencies are often high, and at the low Reynolds numbers involved the boundary layer thickens too rapidly for the classical treatment of forced or mixed convection heat transfer to be valid; in any case, uncertainties remain in boundary layer theory for variable property problems such as those with which we are concerned here. Additionally, the geometry of the heat transfer surfaces may not be simple, again rendering approximate analytic approaches difficult.

There is thus a well-recognized need for numerical methods which are sufficiently powerful and flexible to encompass the phenomena and conditions outlined above. With the rapidly increasing power-to-cost ratio of computers, their use in process analysis and design is becoming ever more attractive. The literature, however, shows very few instances where numerical solutions of the present class of problems have been tested against careful experimental results. Experimental validation is particularly important in view of the frequent absence of a rigorous theoretical basis for the numerical techniques required to treat the relevant differential equations, which may be highly nonlinear, and of mixed type.

The twin objectives of the present work are therefore, on the one hand, to establish an experimental technique for the precise and detailed measurement of local heat transfer coefficients, and on the other, to compare measurements with numerical predictions for a range of conditions. Numerical results are obtained using the finite element method, chosen for the convenience with which it can be applied to problems of irregular and various geometries and the ease with which variable physical properties and rheology can be taken into account. A brief outline of the numerical scheme is included in the present paper, and a more detailed account will be given separately. In the following sections the development of the experimental method is described, followed by a brief account of the numerical methods. Representative results are then compared with numerical predictions for heat transfer in forced and mixed convection to viscous Newtonian and non-Newtonian liquids.

By validating experimental and numerical results against each other, we establish confidence in an experimental technique which can be used to investigate heat transfer to a range of materials in a number of fairly simple geometrics, and a numerical method which is applicable to an infinite variety of geometries.

2. EXPERIMENTAL EQUIPMENT AND PROCEDURES

2.1. *Design considerations for the heat transfer element*

Considerations in choosing the design of the heat transfer element are as follows. Velocity and temperature fields should be two-dimensional over the main part of the element, so that two-dimensional

†Present address: Lloyds Register of Shipping, 29 Wellersley Road, Croydon, Surrey, U.K.

NOMENCLATURE

b	temperature coefficient for viscosity (or consistency), $(-1/\mu)\,\mathrm{d}\mu/\mathrm{d}T$ [K^{-1}]
C	specific heat capacity [J kg^{-1} K^{-1}]
f_i	Cartesian component of the body force [N m^{-3}]
g_i	acceleration due to gravity, Cartesian component [m s^{-2}]
h	local value of heat transfer coefficient, $\{-k(T_s)\,[\partial T/\partial x_2]_s/(T_s-T_\infty)\}$ [W m^{-2} K^{-1}]
J	the Jacobian matrix [m]
k	thermal conductivity [W m^{-1} K^{-1}]
L	length of surface in the direction of flow [m]
m	index in equation (10)
N_I	finite element shape function for node I (biquadratic, isoparametric)
Nu_{x_1}	Nusselt number (local), $(h\,x_1)/k$
n	index in power-law equation for rheology
P_I	$u_i N_{I,i}$ used in forming the SUPG weight function [s^{-1}]
P_Λ	approximate pressure provided by the penalty formulation [N m^{-2}]
p	pressure [N m^{-2}]
q	surface heat flux [W m^{-2}]
R_E	ohmic resistance of heat transfer element [Ω]
Re	tube Reynolds number
Re_L	Reynolds number in terms of length of plate surface
Re_{x_1}	Reynolds number in terms of distance x_1 from leading edge
r	radial distance from the centre of the tube [m]
$\dot{S}$	heat source [W m^{-3}]
T	temperature [K]
T_0	reference temperature in temperature-dependent power-law model [K]
T_{app}	approach temperature, the uniform fluid temperature upstream of the heated plate [K]
T_s	local value of surface temperature [K]
u	velocity vector [m s^{-1}]
u_i	Cartesian coordinate of velocity [m s^{-1}]
u_{iJ}	nodal value, at node J, of the i component of velocity [m s^{-1}]
x_1	distance from leading edge, parallel to surface (i.e. in direction of flow) [m]
x_2	distance perpendicular to surface [m].

Greek symbols

β	a large constant, which multiplied by viscosity gives the penalty parameter
ε	specific electrical conductivity [Ω^{-1}]
Γ	boundary of the finite element analysis domain [m]
$\dot{\gamma}$	shear rate, $[0.5\,\dot{\gamma}_{ij}\,\dot{\gamma}_{ji}]^{1/2}$ [s^{-1}]
$\dot{\gamma}_{ij}$	Cartesian rate of deformation tensor, $(u_{i,j}+u_{j,i})$ [s^{-1}]
Λ	penalty parameter [N s m^{-2}]
λ_ξ	optimal parameter used in forming Φ in the SUPG formulation [m]
λ_η	optimal parameter used in forming Φ in the SUPG formulation [m]
μ	viscosity of fluid [N s m^{-2}]
μ_0	coefficient of consistency in power-law equation for rheology [N s^n m^{-2}]
Φ	upwinding parameter in the SUPG treatment of the momentum conservation equation [s]
ρ	density of fluid [kg m^{-3}]
ξ	finite element local coordinate
η	finite element local coordinate
τ_{ij}	Cartesian viscous stress tensor [N m^{-2}]
χ	upwinding parameter in the SUPG treatment of the energy conservation equation [s]
Ω	the open domain of the finite element analysis [m^2]
Ω_e	the open area of element e [m^2].

modelling can be used. Computer solution of three-dimensional problems is very expensive, and additionally, the acquisition of experimental data defining three-dimensional fields is laborious. Although the computer simulations are not limited to particular geometries, a simple geometry is in practice desirable, if only because it permits a comparison of the results with those obtained from approximate analytical solutions. Furthermore, it should be possible to acquire experimental heat transfer results rapidly. The element should have low thermal mass, equilibrating quickly, and heat transfer coefficients should be obtainable as directly as possible, using relatively few measurements.

These considerations lead to the choice of a flat plate element, which provides a geometry that has frequently been used before in investigations of boundary layer theory. There are two idealized versions—constant surface-temperature, and constant surface-heat-flux plates—and the relative merits of these are now reviewed. The previous investigations which are cited have been selected because of their particular relevance or recent date.

Constant surface-temperature elements have been constructed using copper or aluminium plates backed by a number of heating elements, controlled separately in response to the output of thermocouples set into the metal plate. For these elements it is difficult

to relate electrical power dissipated to local heat flux from the plate surface, because of the finite size of the heating elements, the occurrence of conduction from one part of the metal plate to another, and significant heat losses from the back and edges of the elements. Most workers have calculated surface heat fluxes from the gradients of temperature profiles measured using fine probes situated in the boundary layer close to the plate surface. As a means of obtaining heat transfer coefficients, this procedure is not only indirect and laborious, but is of limited accuracy because of the difficulty of extrapolating the temperature profile right up to the surface. Constant temperature plates, with their heaters and insulated backing, tend to be rather massive, and Ramachandran *et al.* [1], who used a large (300×1040 mm) plate, mention an equilibrium time of 4 h; Reilly *et al.* [2] (150×300 mm) mention times up to 25 min.

In constant heat-flux plates, electric heating elements have provided the heat transfer surfaces. In work by Richardson and co-workers [3], the heating element was in the form of a straight wire, a wire wound on to a former, or a foil glued to a former. At steady state all the electrical power passed from the surface into the fluid, and an average surface temperature was very conveniently obtained from the resistance of the element; the corresponding power dissipation could be determined from measured values of the applied potential difference. The heat transfer coefficient was then obtained from the slope of the linear plot of (applied voltage)^2 vs surface temperature. The method thus yields average heat transfer coefficients over the surface.

In an alternative arrangement, which enables local heat transfer coefficients to be obtained, the heating element is in the form of a foil or shim of high resistance metal such as stainless steel, the local temperatures of which are measured with thermocouples. Sammakia *et al.* [4] used this construction, and used a probe to give boundary-layer temperature profiles. Siebers *et al.* [5] sandwiched thermocouples between stainless steel strip heaters and their substrate, insulating them from the heaters by mica sheet. Dale and Emery [6] ensured direct measurement of the heater temperatures by spot welding thermocouples to the back of the stainless steel shim. Sammakia's element was double-sided, with heat produced symmetrically about a mid-plane, thus eliminating the problem of back heat-losses and the need for bulky insulation.

Elements of the uniform heat-flux type can thus be constructed with low thermal mass. They provide values of local heat transfer coefficients from directly measured local surface temperatures of the plate and a knowledge of the electrical power dissipation; for a properly designed element the latter requires no correction for stray heat losses. This is the design basis for the element used in the present work.

2.2. *Construction of the heat transfer coefficient*

The element was formed from a thin, flat sheet of phenol-formaldehyde (Tufnol) resin covered on both faces by a continuous single strip of stainless steel foil. Heavy current leads and fine potential tappings were connected to the sides of the stainless steel strip, and a number of chromel–alumel thermocouples were spot-welded to the back of the foil on one face. The element was mounted vertically, on stainless steel rods, and the overall arrangement is shown in Fig. 1. Fabrication details were as follows.

The Tufnol plate was prepared with 2 mm diameter holes drilled through it at the thermocouple locations, and with grooves running horizontally from these to the plate edge. A series of 1 mm holes on a 5 mm grid were also drilled, to permit the escape of excess adhesive when fixing the foil to the test face. The precision stainless steel foil (type 302, thickness 0.05 mm $\pm$ 2%, resistivity approximately 90×10^{-8} Ω mm, Goodfellow Metals Ltd) was first fixed over the test face using the epoxy resin (Araldite type 2004, Ciba Geigy Ltd). The thermocouple wires, 0.2 mm in diameter, which were spot-welded through the holes to the back of the foil, were led along the grooves to the edge of the element. The holes and grooves were then filled with an electronics resin (Araldite CY1301/HY1300). Finally, the foil was stuck to the reverse face of the element to give a 'sandwich' 3 mm thick. The current and potential leads were already attached to the foil before it was fixed to the Tufnol. This was done by crimping the leads in an aluminium tube which was then spot-welded to the foil at a large number of points.

With care it was possible to produce an element with flat, smooth surfaces and a neat, square leading edge. For forced and mixed convection heat-transfer experiments the element was mounted in a vertical section of glass QVF tube, of 104 mm internal diameter through which liquid was pumped in an upwards direction. The electric current flowed from side to side through the foil in a direction at right-angles to the fluid streamlines. The rods supporting the element passed through an aluminium collar held between sections of QVF tube, and the electrical leads and thermocouple wires were led out at this point.

The dimensions chosen for the element represent a compromise between several requirements. A wide, low element will maximize its electrical resistance, avoid the need for too-heavy heating currents, and facilitate accurate potential-drop measurements. However, the width is limited by the diameter of the containing tube, and the height should be as great as possible to maximize the range of plate Reynolds numbers attainable. In the final design the height is about 0.9-times the tube internal diameter, so, to maintain laminar flow, experiments were limited to a plate Reynolds number of about 2×10^3. On the basis of the predicted boundary layer thicknesses, and taking note of the work of Hansen [7] and of Elias [8], it was believed that, with the chosen width of element, essentially two-dimensional heat transfer conditions would be achieved over a central region. This was later confirmed by measurement. With an element

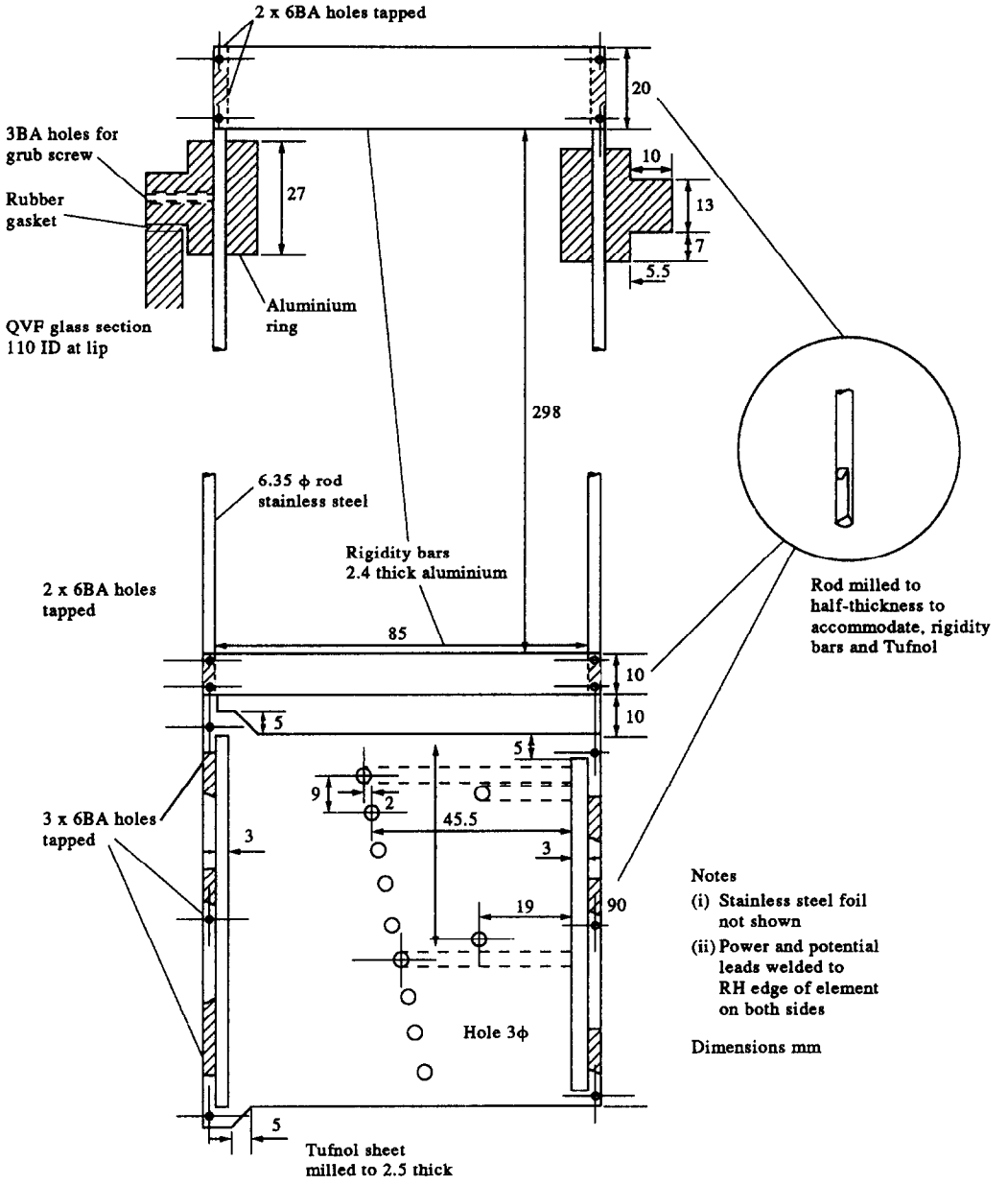

FIG. 1. Heat transfer element and supporting structure.

width of 79 mm, some interaction with the tube walls is inevitable, but again this was shown not to disturb the two-dimensional nature of the heat transfer over the central, test section of the plate.

The layout of the thermocouples on the test face of the element requires brief comment. The main thermocouples are off-set slightly, one behind the other, near the vertical centre line of the element. This is to prevent any flow disturbance resulting from the slight surface irregularities caused by the spot-welding from affecting downstream thermocouples. Two additional thermocouples are positioned 20.5 mm from the element centreline to provide a direct check that the surface heat transfer is two-dimensional.

In order to record bulk fluid temperatures a thermocouple was positioned level with the element, but sufficiently far from its surface to be unaffected by the thermal boundary layer.

2.3. *Power circuit: electrical measurements and calibrations*

In preliminary experiments where DC current was supplied to the heat transfer element, it was found that the surface thermocouple outputs changed by up to 200 μV on reversing the polarity of the supply. This change was comparable with the potential drop expected over the length of foil covered by the thermocouple spot weld, and reliable results could be

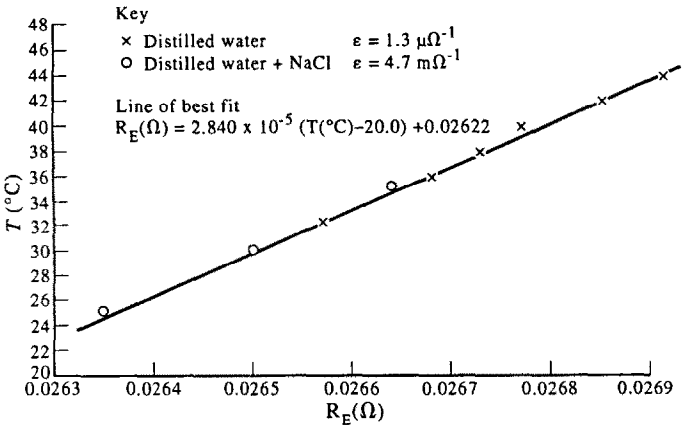

FIG. 2. Electrical resistances of the heat transfer element as a function of temperature.

obtained only by averaging the thermocouple outputs for the two directions of current flow. This, however, was a cumbersome procedure, and the DC supply was replaced by AC obtained from the mains via a step down transformer and Variac. The output from the ungrounded thermocouples, relative to an ice junction, was then measured with a precision of 1 μV using a Solartron 7043 multimeter, which was capable of integrating out the AC component of the signal. Thermocouples were individually calibrated after construction of the heat transfer element.

The potential drop across the element was measured using a Solatron LM 1240 multimeter. The element resistance was initially determined as a function of temperature, and the results are shown in Fig. 2. An experiment was also carried out to test for possible current by-passing when the element is immersed in a conducting liquid. Figure 2 shows resistances measured with the element immersed in distilled water, specific conductivity $\varepsilon = 1.3\ \mu\Omega^{-1}$, and in a salt solution, $\varepsilon = 4.7\ \text{m}\Omega^{-1}$. The points lie indistinguishably on the same resistance–temperature line, and it is therefore concluded that no significant current by-passing occurs.

2.4. *Liquid circulation, flowrates and laser anemometry*

Liquid was pumped, by means of a single stage centrifugal pump, via a flow straightener and distributor, up the vertical column (QVF—104 mm diameter by 3 m tall) containing the heat transfer element and thence back to the holding tank, as shown in Fig. 3. The tank held $50–70 \times 10^{-3}$ m^3 of liquid, with the temperature regulated by adjustment of the flow of cooling water through coils immersed in the tank. The flow rate of the test liquid was controlled by adjustment of the valves in the main flow circuit and in the by-pass line. Both rotameters and an electromagnetic flowmeter were incorporated in the flow loop. The electromagnetic flowmeter was initially calibrated against the rotameters using water, and was subsequently employed as the principal means of controlling and recording liquid flowrates during the heat transfer experiments.

The heat transfer element was mounted vertically across a diameter of the column so that its surface was parallel to the direction of flow. It could be raised or lowered over a span of 0.27 m.

Although the flow-straightener and distributor produced a reasonably uniform flow, the velocity profile was not quite flat, and it was therefore directly measured in the neighbourhood of the element by laser Doppler anemometry. The equipment (Dantec Ltd) incorporated a 35 mW helium–neon laser, and was used in forward-scatter mode. Traversing was achieved by mounting the laser and emitting optics on a rigid bench held in a heavy compound vice. The probe element of the system was approximately 1 mm across the largest dimension. No special seeding of the liquids was necessary. Further details of the use of the laser anemometer are provided elsewhere in ref. [9]. Typical velocity profiles are shown in Fig. 4.

2.5. *Experimental liquids and their characterization*

2.5.1. *Aqueous glycerol.* Two solutions of about 65% wt glycerol were used. Viscosities were measured over the range 20–40°C with U-tube viscometers, and densities were obtained using a specific gravity bottle. Viscosity was well represented by an exponential temperature dependence, and volume expansivity by a linear one. Results are summarized in Table 1. Data for thermal conductivity and its (linear) temperature dependence were taken from the work of Bates [10], whilst specific heats were obtained from the results of Bridgeman [11].

2.5.2. *Aqueous carboxymethyl cellulose solutions.* Solutions of approximately 1.3% wt sodium carboxymethyl cellulose (Grade MR, Hercules Powder Co.) were used. Values of physical properties of CMC solutions have been reported by several workers [2, 12, 13] and, on the basis of this work, the relevant

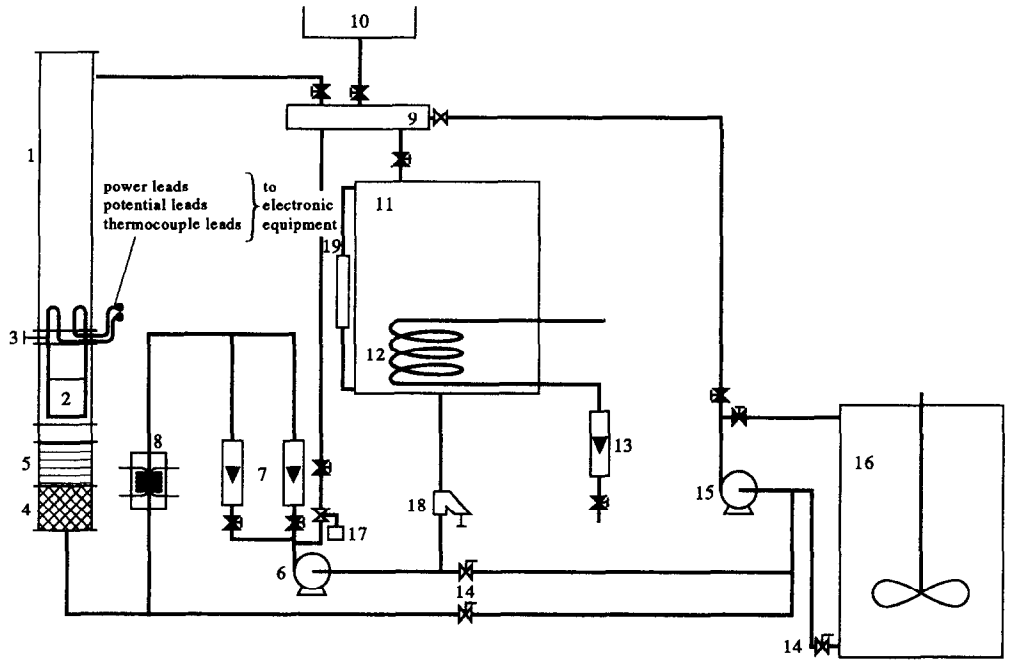

FIG. 3. Liquid flow circuit—1. Column; 2. heat transfer element; 3. element support; 4. flow straightener; 5. flow distributor; 6. single-stage centrifugal pump; 7. rotameters for test fluid; 8. electromagnetic flowmeter; 9. manifold; 10. alternative charging tank; 11. holding tank; 12. cooling coils; 13. cooling water rotameter; 14. drainage cocks; 15. charging pump; 16. storage tank; 17. safety valve; 18. filter; 19. level sight glass.

physical properties, other than rheology, have been taken as those of water at the appropriate temperature. Rheological properties were measured with an R14 Weissenberg rheometer equipped with a Mooney combined truncated cone/concentric cylinder system enclosed in a thermostatically controlled air bath. Results, interpreted in terms of the power-law model, are given in Table 2, from which it will be seen that deviations from Newtonian behaviour are very small.

2.5.3. *Aqueous Carbopol solutions.* Four solutions of carboxy polyethylene (Goodrich Chemical Co., Grade M) were used, and again the physical properties, other than rheology, which was determined as for CMC, were taken to be the same as those of water. Rheological properties are summarized in Table 3, from which it is seen that the solutions are shear-thinning, following the power-law with an exponent ranging from 0.53 to 0.57.

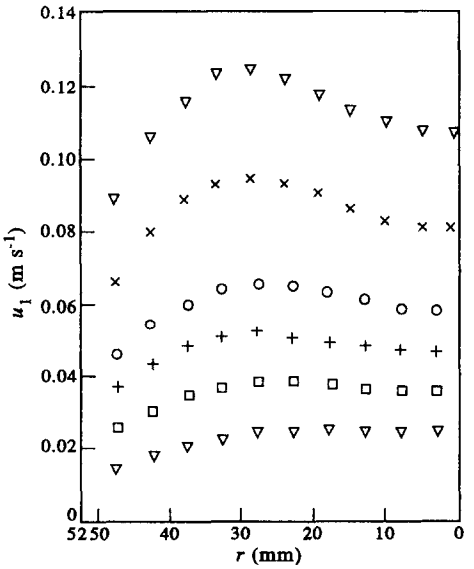

FIG. 4. Typical approach velocity profiles for several experiments; data points from laser doppler anemometry.

2.6. *Experimental procedure*

Liquid was circulated through the equipment at the desired rate and ample time was allowed for steady-

Table 1. Summary of the physical properties of 67.5 and 63.9% aqueous glycerol solutions

Physical Property $T = 20°C$	67.5% Glycerol	63.9% Glycerol
k (W m^{-1} K^{-1})	0.360	0.371
Temp. coeff. (W m^{-1} K^{-2}) $\times 10^3$	−0.250	−0.320
C (J kg^{-1} K^{-1})	3040	3098
ρ (kg m^{-3})	1174	1165
Temp. coeff. (kg m^{-3} K^{-1})	−0.550	−0.563
μ (N s m^{-2})	0.0177	0.0139
Temp. coeff. b (K^{-1}), exponential	0.0430	0.0415

Table 2. Summary of rheological data for the aqueous CMC solutions

Fluid	Temp. (°C)	μ_0(N s^n m^{-2})	n
No. 1 CMC after heat transfer expts	19.3	0.0624	0.985
	25.9	0.0516	0.974
	27.5	0.0446	1.002
	31.2	0.0395	0.998
No. 1 CMC before heat transfer expts	23.7	0.0568	1.010
	31.3	0.0405	0.987
No. 2 CMC	21.9	0.0640	1.007
	24.5	0.0616	1.001
	26.5	0.0553	0.995
	29.3	0.0484	0.985
	30.6	0.0476	0.976

state temperature conditions to be established before any experimental measurements were made. This amounted to about 30 min from initial start-up, or about 15 min following a change of circulation rate. Liquids were replaced when they had become contaminated, and, with those showing shear-degradation (Carbopol solutions), samples were taken at regular intervals and their rheology checked.

Before power was supplied to the element, thermocouple readings were taken, in order, starting from the leading edge, and finally the thermocouple in the bulk liquid was read. When readings had become stable, velocity profiles were measured using the LDA method. Power was then supplied to the element and, after equilibration, the outputs of the element thermocouples were again measured. The rise in temperature of the plate surface was obtained from the difference in the two readings (before and after power was supplied) for each thermocouple. The bulk temperature of the liquid was again measured by the thermocouple situated close to the heat transfer surface.

The total power input to the element was calculated from the applied voltage and the resistance of the element at the mean temperature given by the plate thermocouple readings.

Experiments were carried out with three Newtonian liquids (two aqueous glycerol solutions and an aqueous CMC solution) and with two shear-thinning liquids (aqueous Carbopol solutions). All of the experiments were carried out in the laminar flow regime; the Reynolds numbers with respect to both the tube wall (Re) and the element (Re_L) did not exceed 2000, and in many cases were substantially lower. Under these conditions the boundary layer is thickening very rapidly as the fluid flows over the surface, and the assumptions in the Prandtl boundary layer are no longer applicable.

3. MATHEMATICAL MODEL AND FINITE ELEMENT TECHNIQUES

3.1. *The mathematical model*

We model the conjugate problem of flow and heat transfer in the process liquid, coupled with electrical heat generation and conduction in the flat plate. Account is taken of the dependence of viscosity on shear rate and temperature, and the thermal properties are also taken to be temperature-dependent. The primary mode of heat transfer is by forced convection, but buoyancy effects are also included so that, where necessary, mixed forced and free convection is modelled.

A steady two-dimensional model is set up—the domain of the analysis being in a plane perpendicular to the plate, and lying along the flow direction.

The governing conservation equations for momentum, mass and energy are thus written in Cartesian coordinates as:

$$\rho u_j u_{ij} = -p_{,i} + \tau_{ij,i} + f_i \tag{1}$$

$$u_{i,i} = 0 \tag{2}$$

$$\rho C u_i T_{,i} = k T_{,ii} + \dot{S} \tag{3}$$

where i, j both take the values 1, 2 and the summation convention applies.

Viscous stresses are given by:

$$\tau_{ij} = \mu \dot{\gamma}_{ij} \tag{4}$$

Table 3. Summary of rheological data for Nos. 5, 6, 7 and 8 Carbopol solutions

Fluid	μ_0 (N s^n m^{-2}) $T_0 = 20$°C	b (K^{-1})	n at $T_0 = 20$°C	pH
No. 5 Carbopol	0.425	0.0243	0.528	7.0
No. 6 Carbopol	0.362	0.0197	0.537	7.1
No. 7 Carbopol	0.322	0.0180	0.554	7.1
No. 8 Carbopol	0.281	0.0211	0.572	7.1

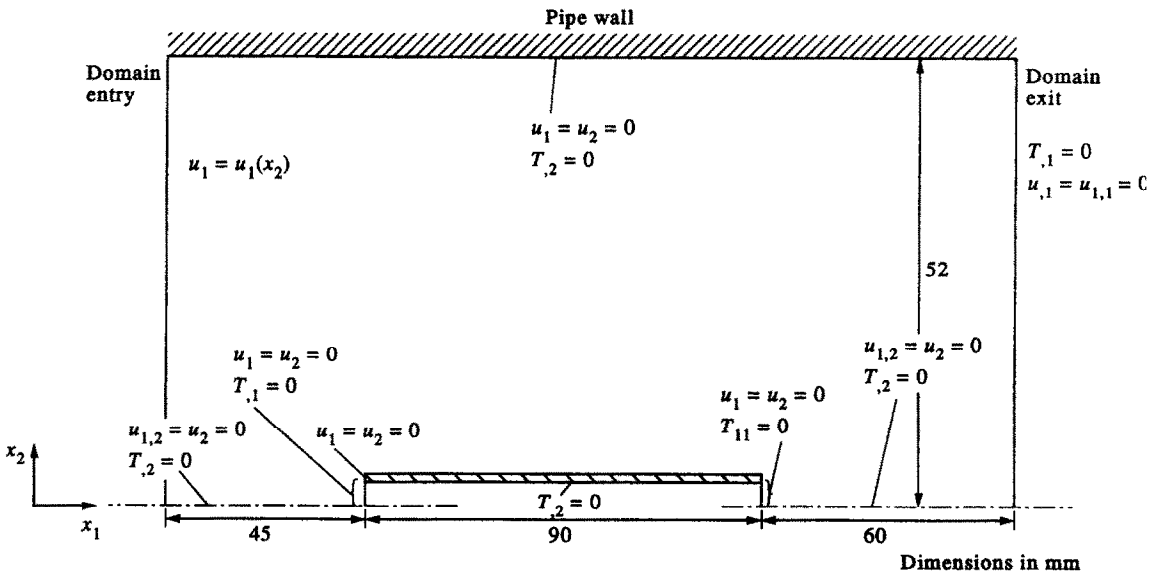

FIG. 5. Domain of the finite element analysis and boundary conditions (plate thickness not shown to scale).

with viscosity expressed in terms of a temperature-dependent power-law equation

$$\mu = \mu_0 \dot{\gamma}^{n-1} e^{-b(T-T_0)}. \quad (5)$$

The body force term represents buoyancy and is written as

$$f_i = [\rho(T) - \rho(T_{app})]g_i \quad (6)$$

where $\rho(T)$ is the density at the local temperature, T, and $\rho(T_{app})$ is the value at the approach temperature, T_{app}. In the continuity equation (2), density is, however, taken as constant. Elsewhere, density, together with thermal conductivity and specific heat, are expressed as linear functions of temperature.

The domain of the analysis is illustrated in Fig. 5; it extends 45 mm upstream and 60 mm downstream from the plate. In the upstream and downstream regions the lower boundary of the domain lies along the symmetry plane of the plate. The domain thus includes the half-thickness of the plate, visible over the central 90 mm of the lower part of the domain. Here, the cross-section of the metal shim, which acts as the electrical heating element, is represented, but not the Tufnol substrate, wherein thermal conduction is negligible. The height of the domain extends to a distance equal to the radius of the pipe in which the element is mounted.

The boundary conditions of the problem are also shown in Fig. 5. Liquid enters in parallel flow across the upstream boundary, with a specified velocity profile $u_1(x_2)$, determined by laser anemometry, and at a specified uniform approach temperature, T_{app}. On the upper boundary, corresponding to the pipe wall, the no-slip condition is specified for the flow, together with zero heat flux across the surface. On the leading and trailing edges of the plate, conditions of no-slip and zero normal heat flux are applied again, whilst the no-slip condition alone is applied to the upper surface of the metal shim (the actual plate surface). On the lower surface of the shim, zero normal heat flux is specified, corresponding to zero heat conduction to or from the Tufnol substrate. On the lower domain boundary, upstream and downstream of the plate, there is symmetry, and corresponding boundary conditions are applied. On the exit boundary, conditions corresponding to kinematically and thermally developed flow are used. Whilst these will probably not apply strictly, their influence on the velocity and temperature fields is exerted over only a short upstream distance, and there is no practical alternative to their use. The downstream 60 mm section of the domain has been chosen to be sufficiently long to ensure that heat transfer near the plate is unaffected by any of the approximations involved in the downstream boundary conditions.

Equations (1)–(3), with equations (4)–(6) etc., are applied over the whole domain. Appropriate physical properties are assigned in the regions representing the flow area and the steel shim. In the steel, the source term, $\dot{S}$, in the energy equation is assigned a value representing the rate of electrical heat generation, and the flow boundary conditions ensure that zero velocities are maintained in the metal. In the flow region, the source term represents heating due to viscous energy dissipation

$$\dot{S} = \mu[(u_{1,1})^2 + (u_{2,2})^2 + 2(u_{1,2} + u_{2,1})^2]. \quad (7)$$

The governing equations provide a detailed representation of the physics, and form a coupled, nonlinear system, which is of mixed hyperbolic–elliptic type as a result of the important convective transfer

terms; the correct solution of this system presents a significant challenge.

3.2. *Finite element techniques*

In this Section, an outline is given of the finite element techniques used to solve the mathematical model that has been described. Some novel aspects are highlighted, and a fuller account will be given elsewhere [14].

The incompressible flow problem is solved using the Reduced Integration Penalty formulation, which removes pressure as a primary unknown using the substitution

$$p_\Lambda = -\Lambda u_{i,i}$$

$$p_\Lambda \to p \text{ as } \Lambda \to \infty.$$

To maintain uniform continuity enforcement, we introduce a viscosity-dependent penalty parameter [15]

$$\Lambda = \beta\mu$$

where β is a large constant, typically 10^8 in 64 bit calculations.

An important consideration in the present work is the proper treatment of momentum and energy transport involving a significant convective component, represented by the first derivative terms in equations (1) and (3). It is well known that when mesh Reynolds or Peclet numbers are not small, $< O(1)$, the classical finite element Galerkin method can lead to worthless, oscillatory results. One of the most effective techniques providing solutions to such problems that are both smooth and accurate, is the Streamline Upwind Petrov Galerkin (SUPG) formulation, proposed by Brooks and Hughes [16]. In its original form, this was described for use with bilinear elements. We wish to take advantage of the greater efficiency and geometrical flexibility of biquadratic elements, and we make use of recent work by Petera *et al.* [17]. This extends SUPG to isoparametric, biquadratic Langrangian elements, and introduces an upwind weighting function structure based on that of Brooks and Hughes, but incorporating optimal upwind parameters for biquadratic elements, proposed by Donea *et al.* [18]. The formulation was tested successfully against analytic solutions for a scalar, constant property convection–diffusion problem [17]. In the present work we apply this formulation, for the first time, to nonlinear equations involving variable physical properties. The resulting finite element equations, corresponding to equation (1) for momentum conservation, are

$$\int [\rho N_I(N_{J,1}N_K u_{1K} + N_{J,2}N_K u_{2K})u_{1J}$$
$$+ \mu(2N_{I,1}N_{J,1} + N_{I,2}N_{J,2})u_{1J} + \mu N_{I,2}N_{J,1}u_{2J}$$
$$+ \beta\mu(N_{I,1}N_{J,1}u_{1J} + N_{I,1}N_{J,2}u_{2J})]\,d\Omega$$
$$+ \sum_e \int_{\Omega_e} \Phi P_I[\rho(N_{J,1}N_K u_{1K} + N_{J,2}N_K u_{2K})u_{1J}$$
$$- \mu(2N_{J,11} + N_{J,22})u_{1J} - \mu N_{J,12}u_{2J}$$
$$- (2\mu_{,1}N_{J,1} + \mu_{,2}N_{J,2})u_{1J}$$
$$- \mu_{,2}N_{J,1}u_{2J} - \beta\mu N_{J,11}u_{1J} - \beta\mu N_{J,21}u_{2J}$$
$$- \beta\mu_{,1}N_{J,1}u_{1J} - \beta\mu_{,1}N_{J,2}u_{2J}]\,d\Omega$$
$$= \int_\Omega N_I f_1\,d\Omega + \int_\Gamma N_I t_1\,d\Gamma + \sum_e \int_{\Omega_e} \Phi P_I f_1\,d\Omega \qquad (8a)$$

and

$$\int_\Omega [\rho N_I(N_{J,1}N_K u_{1K} + N_{J,2}N_K u_{2K})u_{2J}$$
$$+ \mu(N_{I,1}N_{J,1} + 2N_{I,2}N_{J,2})u_{2J} + \mu N_{I,1}N_{J,2}u_{1J}$$
$$+ \beta\mu(N_{I,2}N_{J,2}u_{2J} + N_{I,2}N_{J,1}u_{1J})]\,d\Omega$$
$$+ \sum_e \int_{\Omega_e} \Phi P_I[\rho(N_{J,1}N_K u_{1K} + N_{J,2}N_K u_{2K})u_{2J}$$
$$- \mu(N_{J,11} + 2N_{J,22})u_{2J} - \mu N_{J,21}u_{1J}$$
$$- (\mu_{,1}N_{J,1} + \mu_{,2}2N_{J,2})u_{2J}$$
$$- \mu_{,1}N_{J,2}u_{1J} - \beta\mu N_{J,22}u_{2J}$$
$$- \beta\mu N_{J,12}u_{1J} - \beta\mu_{,2}N_{J,2}u_{2J} - \beta\mu_{,2}N_{J,1}u_{1J}]\,d\Omega$$
$$= \int_\Omega N_I f_2\,d\Omega + \int_\Gamma N_I t_2\,d\Gamma + \sum_e \int_{\Omega_e} \Phi P_I f_2\,d\Omega \qquad (8b)$$

and, corresponding to equation (3) for energy conservation

$$\int_\Omega [\rho C N_I(N_K N_{J,1}u_{1K} + N_K N_{J,2}u_{2K})$$
$$+ k(N_{I,1}N_{J,1} + N_{I,2}N_{J,2})]\,d\Omega\,T_J$$
$$- \sum_e \int_{\Omega_e} \chi P_I[\rho C(N_K N_{J,1}u_{1K} + N_K N_{J,2}u_{2K})$$
$$- k(N_{J,11} + N_{J,22}) - (k_{,1}N_{J,1} + k_{,2}N_{J,2})]\,d\Omega\,T_J$$
$$= \int_\Omega N_I \dot{S}\,d\Omega - \int_\Gamma N_I q_n\,d\Gamma + \sum_e \int_{\Omega_e} \chi P_I \dot{S}\,d\Omega. \qquad (9)$$

Here, the weighting functions in this consistent weighted residual statement are $(N_I + \Phi P_I)$ in equation (8) and $(N_I + \chi P_I)$ in equation (9), where N_I is the usual C^0 continuous shape function, and

$$P_I = u_i N_{I,i}.$$

This part of the function is therefore discontinuous across element boundaries, and terms weighted by it are evaluated on element interiors, without the application of integration by parts. As a consequence, second derivatives of the shape function N_I with respect to Cartesian coordinates remain in the formulation. How to evaluate these is not immediately obvious, but in previous work [17] we have proposed convenient, exact formulae for the purpose. An

additional complication, not previously considered, arises from the variability of the physical properties, which leads to the occurrence of Cartesian derivatives of viscosity and thermal conductivity in equations (8) and (9). These need to be evaluated at integration points, and for viscosity we obtain them via the derivatives with respect to element local coordinates, (ξ, η), calculated from second-order finite difference formulae based on the 3×3 integration points in the biquadratic elements. For example, the ξ derivative of viscosity, $\mu_{,\xi}$, at the integration point with local coordinates (0,0), is given by

$$\mu(0,0)_{,\xi} = \frac{\mu(\xi_G,0) - \mu(-\xi_G,0)}{2\xi_G}$$

where $\xi_G = 0.7745966692$, and similarly at other integration points, using central or one-sided finite difference formulae, as appropriate. The required Cartesian derivatives are then calculated from

$$\begin{bmatrix} \mu_{,1} \\ \mu_{,2} \end{bmatrix} = J^{-1} \begin{bmatrix} \mu_{,\xi} \\ \mu_{,\eta} \end{bmatrix}$$

where J^{-1} is the inverse of the Jacobian matrix

$$J = \begin{bmatrix} x_{1,\xi} & x_{2,\xi} \\ x_{1,\eta} & x_{,\eta} \end{bmatrix}.$$

The upwinding parameter, Φ, is constructed by blending terms corresponding to the local coordinate components of the velocity vector, as

$$\Phi = \frac{|\lambda_\xi| u_\xi^2 + |\lambda_\eta| u_\eta^2}{|u|^2} \frac{1}{|u|}$$

where the λ_ξ and λ_η are parameters (with dimensions of length) evaluated 'optimally' as functions of the local mesh Reynolds number and element dimensions, as explained in ref. [17]. The parameter χ is evaluated in a corresponding way, based on mesh Peclet number.

The nonlinearity of the problem is treated using a successive substitution iterative scheme; the equations are linearized using physical property values, and velocities in the inertia terms, corresponding to the solution obtained in the previous iteration. The procedure is started using a Newtonian, isothermal, creeping flow solution. Whilst this is a rather low order iterature scheme, it has been found to be robust for high degrees of nonlinearity.

The linearized finite element equations are solved by the 'frontal' method.

3.3. *Implementing the finite element solutions*

A finite element mesh of the type used in the present work is shown in Fig. 6. The results presented in the next section were obtained using a somewhat more refined mesh, which, on the basis of extensive mesh refinement experiments, is believed to provide effectively converged results. This refined mesh, containing 5115 nodes, is not shown, since the very small elements in some areas would coalesce. The mesh design is guided by approximate estimates of the thermal boundary layer thickness from classical boundary layer theory, with increasing mesh refinement near the plate surface, and near leading and trailing edges.

The stainless steel shim is represented in a single layer of very thin elements, wherein the physical properties of steel are assigned, and where the source term, $\dot{S}$ (W m^{-3}), in equation (3) is set to a value representing the electrical heating power. Initial results showed, not surprisingly, that the use of elements only 0.05 mm thick (the actual shim thickness) caused numerical problems. The thickness of the elements representing the shim was therefore increased five-fold, with a five-fold reduction in the assigned values of thermal conductivity and thermal source term, thus maintaining the proper flow-direction thermal conduction in the shim, and the correct electrical power input.

Solutions typically required 7–15 iterations for convergence, depending on the degree of nonlinearity—increasing importance of the buoyancy term, in particular, necessitated larger numbers of iterations. The convergence criterion for velocities took the form

$$\frac{\sum_I (u_I^{n+1} - u_I^n)^2}{\sum_I (u_I^{n+1})^2} \leqslant 10^{-5}$$

where n is the iteration counter; the corresponding criterion for nodal temperatures was also applied.

4. DISCUSSION AND CONCLUSIONS

The work reported here covers an extension and refinement of that presented at a recent conference [19]. The experimental programme, which is reported in detail elsewhere [9] included 116 experimental determinations of temperature profiles along the plate and covered the use of three Newtonian fluids (an aqueous CMC solution and glycerol–water mixtures of 67.5 and 63.9 w/w concentrations) and one shear-thinning fluid (aqueous Carbopol) with a power-law index of approximately 0.5. Approach velocities ranged from 0.018 to 0.26 m s^{-1} ($14\times$ variation) and heat fluxes from 0.10 to 20.7 kW m^{-2} ($207\times$).

Numerical solutions of the coupled flow and heat transfer problem were carried out to give plate temperature profiles for the conditions applying in seven experiments, which were representative of those in the overall programme. In this way, it was possible to make a direct comparison of computed and measured temperatures. Results are given in Figs. 7–13, from which it is seen that the agreement is such as to give a high degree of confidence in both the experimental and the computational procedures. Reference should be made to Table 4 for experimental conditions. In Figs. 7–9, two computed curves are shown—one for combined forced and natural convection and the other for forced convection alone (i.e. with the buoyancy effects arising from density variations neglected). As would be expected, the effects of buoyancy are greatest

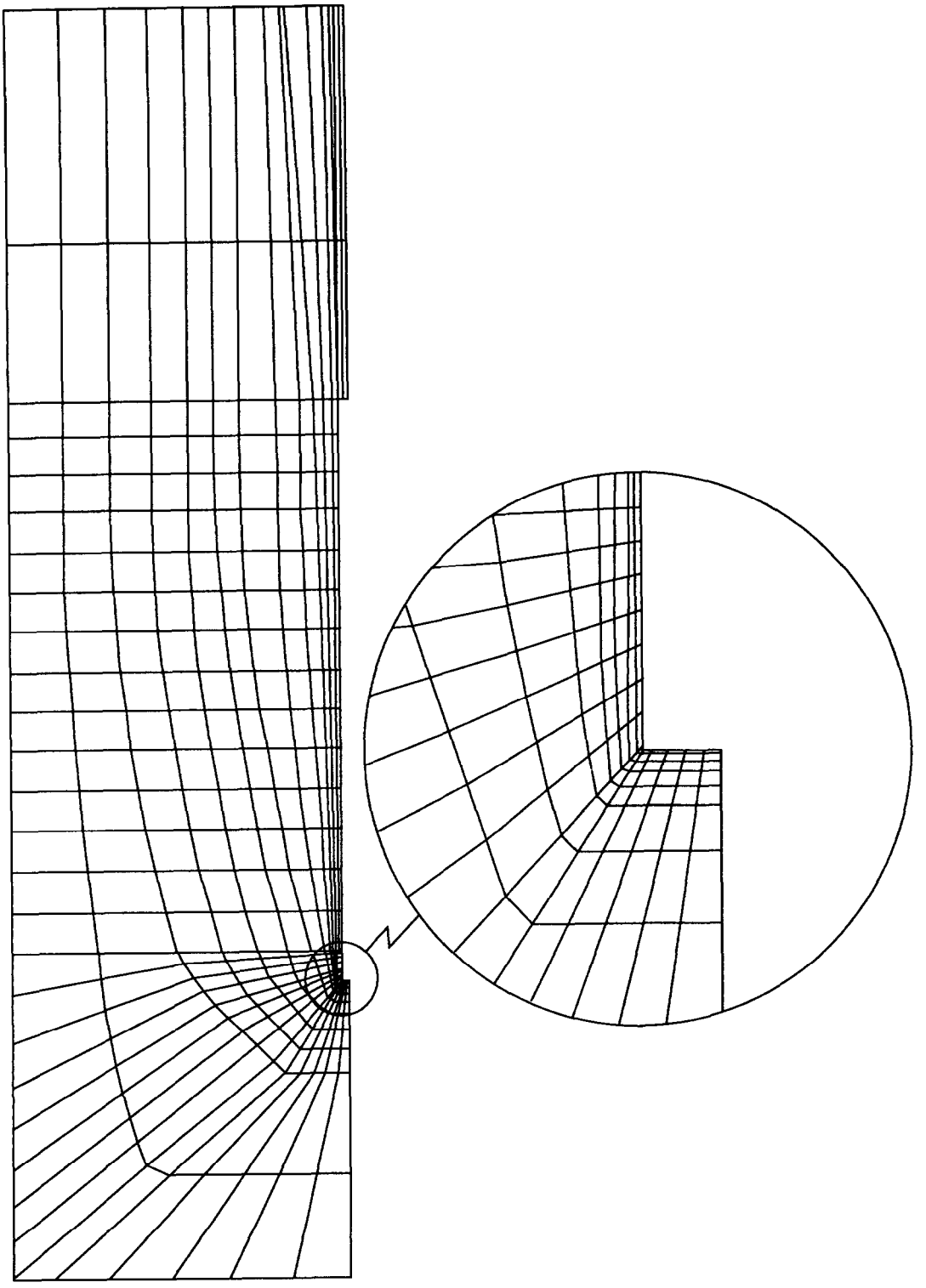

FIG. 6. Finite element mesh.

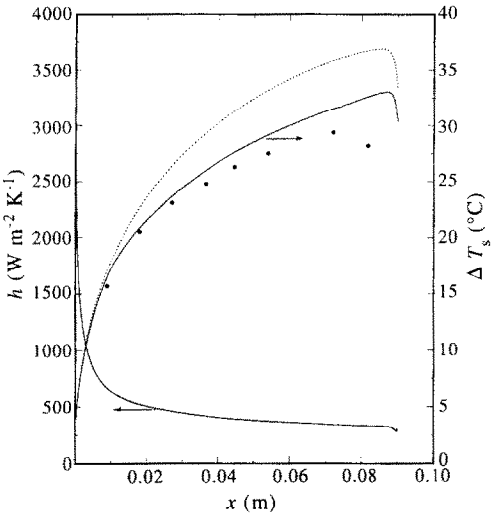

FIG. 7. Experimental •, computed temperature profiles —— and local heat transfer coefficients. Computed results neglecting buoyancy effects – – – (experiment 7—aqueous CMC).

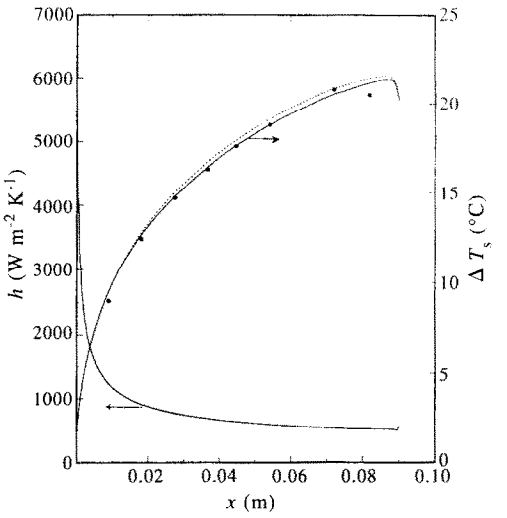

FIG. 9. Experimental •, computed temperature profiles —— and local heat transfer coefficients. Computed results neglecting buoyancy effects – – – (experiment 47).

at high heat fluxes and lower plate Reynolds numbers, and closer agreement with the experimental results is obtained if the effects of natural convection are included. In order to assess the magnitude of the overall effect of variations of physical properties, temperature profiles were also computed in one experiment (Fig. 13), on the assumption that all properties remained equal to those at the approach temperature. The results indicate the importance of taking these variations into account in the computations.

A further set of curves included in Figs. 7–13 gives the value of the local heat transfer coefficient h. Although the plate heat transfer element was nominally of the constant heat flux type, there were local variations of normal heat flux at the surface due to the conduction of heat through the foil in the upstream direction, this effect being greatest near the leading edge where $\partial T/\partial x_1$ was a maximum. Excluding regions within about 1 mm of the leading and trailing edges, the maximum variation in surface normal heat flux was approximately 5%.

The local values of heat transfer coefficients given in Figs. 7–13 were therefore computed as

$$h = \frac{\text{Local heat flux normal to surface}}{\text{Difference between surface and bulk temperatures}} = \frac{-k(T_s)\left(\dfrac{\partial T}{\partial x_2}\right)_s}{T_s - T_{app}}$$

where suffix s refers to the condition at the surface. For the Newtonian fluids the computed values of the local heat transfer coefficient were then examined in

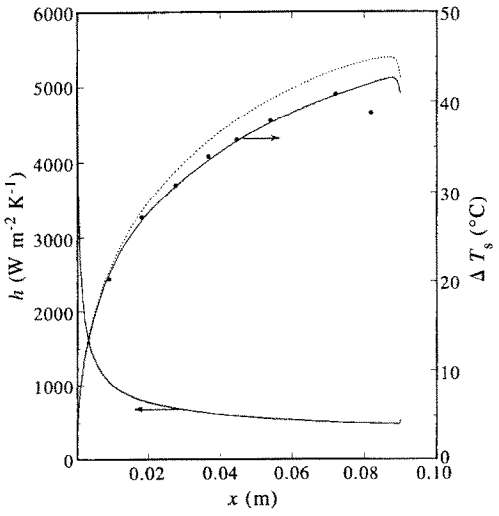

FIG. 8. Experimental •, computed temperature profiles —— and local heat transfer coefficients. Computed results neglecting buoyancy effects – – – (experiment 33).

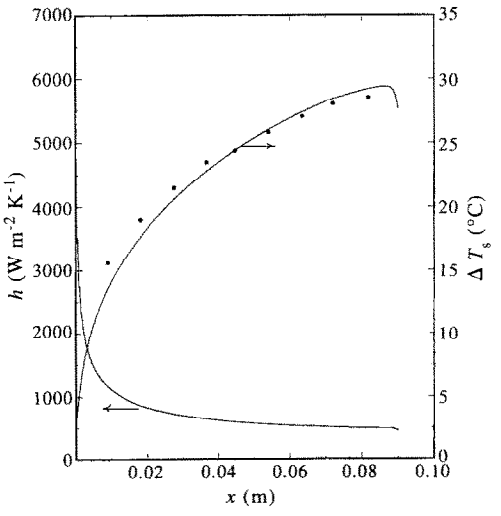

FIG. 10. Experimental •, computed temperature profiles —— and local heat transfer coefficients (experiment 65).

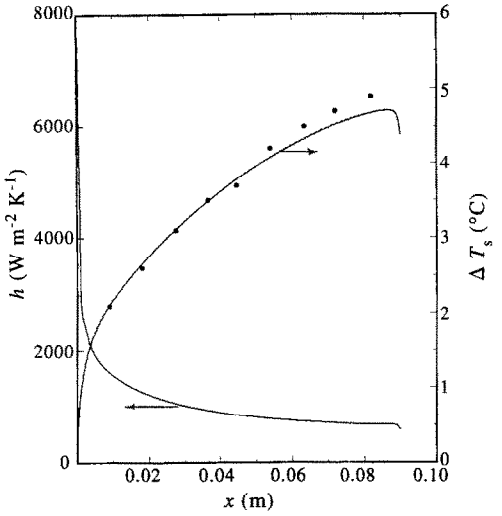

FIG. 11. Experimental •, computed temperature profiles —— and local heat transfer coefficients (experiment 80).

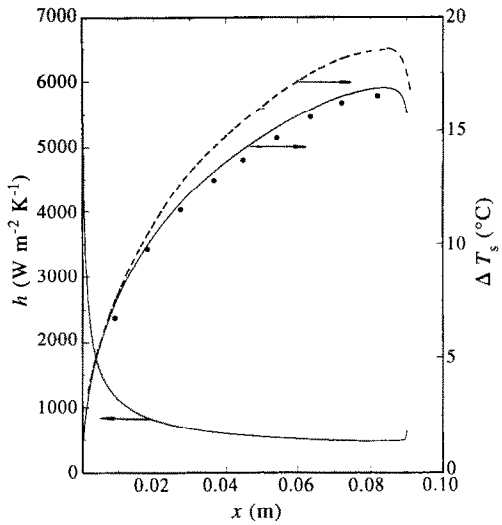

FIG. 13. Experimental •, computed temperature profiles —— and local heat transfer coefficients (experiment 101). Broken line—all physical properties assumed constant.

terms of local Nusselt number as a function of local Reynolds number, using the physical property values applicable to the approach temperatures. It was not possible to correlate the results for the various fluids used in the experiments by means of a single value of the Prandtl number in each case, because of the point-to-point variations attributable to the temperature-dependence of physical properties. However, in order to obtain a general comparison of the results for different systems, a simple function of Prandtl number was employed, $Pr^{1/3}$, in which physical property values are evaluated at the approach temperature. The results for the non-Newtonian fluids were excluded from the correlation because of the even greater difficulty in relation to the appropriate definition of a relevant Prandtl number.

In view of the fact that logarithmic plots of Nu_{x_1} vs Re_{x_1} were approximately linear for all x_1-positions,

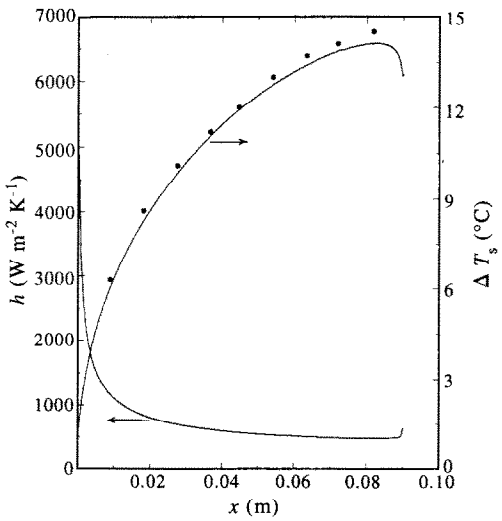

FIG. 12. Experimental •, computed temperature profiles —— and local heat transfer coefficients (experiment 94).

except those very near to the leading and trailing edges, it was then possible to express the results for each experiment in the form

$$Nu_{x_1} = K\,Re_{x_1}{}^{m}\,Pr^{1/3}. \tag{10}$$

The values of K and m are given in Table 4.

In Fig. 14, a logarithmic plot of $Nu_{x_1}\,Pr^{-1/3}$ vs Re_{x_1} is shown for each of the Newtonian fluids for which computed results have been obtained. In addition, the line representing results predicted from the equation based on the simple boundary layer theory is shown. For the constant heat flux condition, this is

$$Nu_{x_1} = 0.451\,Re_{x_1}{}^{1/2}\,Pr^{1/3}. \tag{11}$$

The slope of this line is somewhat smaller than that for the computed lines, being 0.5 compared with ~0.6.

Although the form of the function describing the computed results is similar to that predicted by the boundary layer theory, the numerical values of the Nusselt numbers differ by a factor of up to 3. This underlines the need for computations in circumstances where the Reynolds numbers are low and where local values of physical properties are sufficiently influenced by temperature to differ significantly from those of the approach fluid. It should be borne in mind that the numerical values of heat transfer coefficient which have been computed refer only to the particular geometry of the heat transfer element used in this work. Even for the plane surface, it would be necessary to include some function of the plate thickness in the correlation above, in order to allow the results to be applied more generally; also, to account for the effects of physical property variations (particularly the temperature-dependence of viscosity and buoyancy effects arising from density variations), further groups would be necessary. In view of this complexity, and the specialized geometry of the problem, no attempt has been made to develop the correlation

Table 4. Values of exponent m and coefficient K in equation (10), with experimental conditions

Experiment No.	Material	Approach velocity (m s $^{-1}$)	Plate Reynolds Number† Re_L	Heat flux (kW m^{-2})	Prandtl No. Pr	m	K
7	Aqueous CMC	0.0179	60	10.90	186	0.670	0.590
33	Aqueous CMC	0.0524	240	20.70	134	0.639	0.520
47	Aqueous CMC	0.0959	230	10.90	285	0.596	0.460
65	67.5% Glycerol	0.0458	960	19.38	49	0.604	0.500
80	63.7% Glycerol	0.1150	1500	1.99	75	0.653	0.310
94	Carbopol 5	0.0791	20	6.66	—	—	—
101	Carbopol 6	0.1030	35	8.57	—	—	—
Boundary layer theory	General	—	—	—	—	0.5	0.451

†Metzner and Reed Reynolds Number for Carbopols

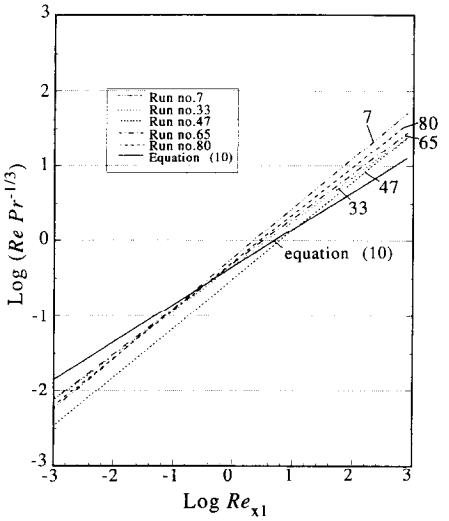

FIG. 14. $Nu_{x_1}\ Pr^{-1/3}$ vs Re_{x_1} correlations.

further. The numerical method provides the means for obtaining accurate details of the heat transfer process in this and many other geometries.

It should be stressed that, so far as the authors are aware, the present work is the first in which the SUPG finite element formulation has been applied, on isoparametric biquadratic elements, to a problem with variable physical properties. In view of the fact that the SUPG formulation for nonlinear, multidimensional problems is based on a heuristic extension of theoretical results derived for simplified one-dimensional cases [17], the present agreement between computation and experiment provides particularly valuable reassurance as to the success of the formulation in providing accurate, stable results.

REFERENCES

1. N. Ramachandran, B. F. Armaly and T. S. Chen, Measurements and predictions of laminar mixed convection flow adjacent to a vertical surface, *Trans. ASME J. Heat Transfer* **107,** 636–641 (1985).
2. I. G. Reilly, C. Tien and M. Adelman, Experimental study of natural convective heat transfer from a vertical plate in a non-Newtonian fluid, *Can. J. Chem. Engng* **7,** 157–160 (1965).
3. J. F. Richardson, M. N. Romani and K. J. Shakiri, Heat transfer from immersed surfaces in liquid fluidised beds, *Chem. Engng. Sci.* **31,** 619–624 (1976).
4. B. Sammakia, V. P. Carey and B. Gebhart, Measurements and calculations of transient mixed convection in air, *Int. J. Heat Mass Transfer* **28,** 1837–1846 (1985).
5. D. L. Siebers, R. F. Moffat and R. G. Schwind, Experimental variable properties natural convection from a large, vertical, flat surface, *Trans. ASME* **107,** 124–132 (1985).
6. J. D. Dale and A. F. Emery, The free convection of heat from a vertical plate to several non-Newtonian pseudoplastic fluids, *Trans. ASME, J. Heat Transfer* **94,** 64–73 (1972).
7. M. Hansen, Velocity distribution in the boundary layer of a submerged plate, *NACA* TM **585.**
8. F. Elias, The transference of heat from a hot plate to an air stream, *NACA* TM **614.**
9. C. P. Sherrard, Heat transfer to Newtonian and non-Newtonian liquids from a vertical flat plate, Ph.D. Thesis, University of Wales, Swansea (1987).
10. O. K. Bates, Thermal conductivity of aqueous glycerol solutions, *Ind. Engng Chem.* **28,** 494–500 (1936).
11. R. Bridgeman, Heat capacities of mixtures of glycerol and water, *Am. Acad. Arts. Sci.* **61,** 101–107 (1926).
12. E. B. Christiansen and S. E. Graig, Heat transfer to pseudoplastic fluids in laminar flow, *A.I.Ch.E. Jl* **8,** 154–160 (1962).
13. J. H. Boggs and W. L. Sibbitt, The thermophysical properties of some low concentration aqueous polymer solutions, *Ind. Engng Chem.* **47,** 289–295 (1955).
14. J. F. T. Pittman, To be published.
15. J. F. T. Pittman, Finite elements for field problems. In *Fundamentals of Computer Modeling for Polymer Processing* (Edited by C. L. Tucker, III), Chap. 6. Carl Hanser, Munich (1989).
16. A. N. Brooks and T. J. R. Hughes, Streamline upwind Petrov–Galerkin formulations for convection dominated flows with particular emphasis on the incompressible Navier–Stokes equations, *Comp. Meth. Appl. Mech. Engng* **32,** 199–259 (1982).
17. J. Petera, V. Nassehi and J. F. T. Pittman, Petrov-Galerkin methods on isoparametric bilinear and biquadratic elements tested for a scalar convection–diffusion problem, *Int. J. Numer. Meth. Heat Fluid Flow* **3,** 205 221 (1993).
18. J. Donea, T. Belytschko and P. A. Smolinski, A generalized Galerkin method for steady convection diffusion problems with application to quadratic shape function elements, *Comp. Meth. Appl. Mech. Engng* **48,** 25 43 (1985).
19. J. F. T. Pittman, J. F. Richardson, A. O. Sharif and C. P. Sherrard, Convective heat transfer from a flat plate with uniform surface heat flux: experimental and computational results, *Inst. Chem. Engrs Symp. Series*, No. **129** (1992).